Journal of Automation and Intelligence 4 (2025) 73–81

Contents lists available at ScienceDirect

Journal of Automation and Intelligence

Research article

Fault-tolerant control of wheeled mobile robots with prescribed trajectory tracking performance☆

Jin-Xi Zhang, Tianyou Chai *

Department of the State Key Laboratory of Synthetical Automation for Process Industries, Northeastern University, Shenyang, 110819, China

ARTICLE INFO

Keywords:
Fault-tolerant control
Prescribed performance
Trajectory tracking
Wheeled mobile robots

ABSTRACT

The problem of trajectory tracking for a class of differentially driven wheeled mobile robots (WMRs) under partial loss of the effectiveness of the actuated wheels is investigated in this paper. Such actuator faults may cause the loss of strong controllability of the WMR, such that the conventional fault-tolerant control strategies unworkable. In this paper, a new mixed-gain adaption scheme is devised, which is adopted to adapt the gain of a decoupling prescribed performance controller to adaptively compensate for the loss of the effectiveness of the actuators. Different from the existing gain adaption technique which depends on both the barrier functions and their partial derivatives, ours involves only the barrier functions. This yields a lower magnitude of the resulting control signals. Our controller accomplishes trajectory tracking of the WMR with the prescribed rate and accuracy even in the faulty case, and the control design relies on neither the information of the WMR dynamics and the actuator faults nor the tools for function approximation, parameter identification, and fault detection or estimation. The comparative simulation results justify the theoretical findings.

1. Introduction

By feat of the high flexibility, efficiency and degree of automation, wheeled mobile robots (WMRs) have been or are being applied in various commercial and military fields where human intervention is slow, expensive, unreliable or infeasible. For instance, the intelligent inspection WMRs constitute a platform for intelligent data collection, decision-making judgment, information integration and inspection, and operation and maintenance of industrial scenarios. For another example, the reconnaissance WMR is used for surveillance, reconnaissance, explosive ordnance disposal, and communications relay. On the other hand, several theoretical challenges inspire the research interest from academia. In general, the WMR is driven in an underactuated mode and exhibits uncertain dynamics, both of which challenge the control design. Motion control is the basic foundation of a WMR, of which trajectory tracking is a typical task, i.e., drive the WMR to move along a spatial and temporal target trajectory. To this end, various control methods have been developed for WMRs, e.g., proportional–integral–derivative control [1], linear–quadratic regulator control [2], model predictive control [3], adaptive control [4], sliding mode control [5], iterative learning control [6], neural network control [7], fuzzy control [8], and prescribed performance control (PPC) [9–12]. In particular, the PPC strategy accomplishes trajectory tracking of the WMR with the preassigned rate, overshoot and accuracy even in the presence of unknown dynamics and external disturbances.

Nonetheless, of particular note is that the above methods work for the fault-free case. In practical applications, WMRs are unlikely ever immune to faults. The long-term operation results in aging, leakage, and wear and tear of the sensors and actuators of the WMR. The temperature, humidity, electromagnetic fields, and vibration in a harsh environment have also an impact on the function and lifetime of these components. For example, the WMR in an open-pit mine is subject to extreme cold or heat, dense dust, and gravel roads; the WMR in a metallurgical industry is exposed to thermal and electromagnetic radiation. Faults may not only cause mission failures but also lead to secondary hazard. Once the WMR goes out of control, it could collide

Peer review under responsibility of Chongqing University.

☆ This work was supported in part by the National Natural Science Foundation of China under Grants 61991404, 62103093 and 62473089, the Research Program of the Liaoning Liaohe Laboratory, China under Grant LLL23ZZ-05-01, the Key Research and Development Program of Liaoning Province of China under Grant 2023JH26/10200011, the 111 Project 2.0 of China under Grant B08015, the National Key Research and Development Program of China under Grant 2022YFB3305905, the Xingliao Talent Program of Liaoning Province of China under Grant XLYC2203130, the Natural Science Foundation of Liaoning Province of China under Grants 2024JH3/10200012 and 2023-MS-087, the Open Research Project of the State Key Laboratory of Industrial Control Technology of China under Grant ICT2024B12, and the Fundamental Research Funds for the Central Universities of China under Grants N2108003 and N2424004.

*

with people or objects in its surroundings. Actuator faults seriously threaten the control system [13], whose dynamic behavior is directly altered by the false control command. Fault-tolerant control (FTC) aims to ensure the control system to retain stable and perform its basic functions in the event of faults.

The WMRs are a type of multivariable nonlinear systems with inputs coupling. For such plants with unknown control distribution matrices (CDMs), most of the existing FTC methods work for the case of the strongly controllable faulty systems. This means that the unknown CDM plus its inverse matrix is uniformly positive or negative definite, even in the presence of actuator faults [14–18]. This requirement can be satisfied for diverse healthy practical systems, such as permanent magnet synchronous motors, marine engineering vehicles, robotic manipulators, etc. In the event of partial loss of effectiveness (PLOE) of the actuators, however, the system CDM is changed and its transformed version may become singular. In this case, just the controllability of the healthy system holds. To eliminate the need for the strong controllability of the faulty WMR, an iterative learning FTC strategy was developed [19], in which the constant inertial matrix of the WMR is skilfully introduced in the Lyapunov candidate function. Nevertheless, it necessitates the known nonlinearities of the WMR and is not effective for the case of the state-dependent CDM [5,8]. Recently, some FTC designs for the non-strongly controllable nonlinear plants were reported [20–22], in which the variable gain technique is adopted to accommodate the actuator PLOE faults. However, the consequent control magnitude may be significantly enlarged, because the variable gain is a lumped term of the norms of two types of barrier functions. It is noteworthy that any barrier function possesses the infinity property.

In this paper, an innovative fault-tolerant PPC strategy based on a novel mixed-gain adaptation technique is devised for the WMRs under unknown dynamics, external disturbances and actuator PLOE faults. It outperforms the above-mentioned FTC methods as summarized below.

1. The requirement for the strongly controllable faulty WMR [14–18] is excluded.
2. It steers the WMR to track the target trajectory with the prespecified rate and accuracy, unlike the uniform ultimate boundedness of the tracking errors [5,8,23–27].
3. It exhibits both a low-gain property compared with [20–22] and a low complexity without parameter identification [4,18,19,24,25,28,29], function approximation [5,7,8,12,23,26,27], disturbance estimation [8,11] or fault estimation [30].

The remainder of the paper is organized as follows. Section 2 formulates the problem under consideration. The control design is carried out in Section 3. Section 4 validates its feasibility. A simulation study is performed in Section 5. Finally, Section 6 concludes this paper.

2. Problem formulation

2.1. System description

Consider the differentially driven WMR illustrated by Fig. 1, whose motion equations are written by [9,19,23,25,31]

$$\begin{cases} \dot{x}(t) = \dfrac{r}{2}(v_1(t)+v_2(t))\cos\theta(t), \\ \dot{y}(t) = \dfrac{r}{2}(v_1(t)+v_2(t))\sin\theta(t), \\ \dot{\theta}(t) = \dfrac{r}{2b}(v_1(t)-v_2(t)), \\ \dot{\boldsymbol{v}}(t) = \boldsymbol{A}(\theta(t),\boldsymbol{v}(t)) + \boldsymbol{B}(\theta(t),\boldsymbol{v}(t))\boldsymbol{\tau}(t) + \boldsymbol{D}(t), \end{cases} \tag{1}$$

where $(x(t), y(t))$ and $\theta(t)$ denote the position and heading of the WMR, respectively; $\boldsymbol{v}(t) = [v_1(t), v_2(t)]^{\mathrm{T}} \in \Re^2$ is a vector of the angular velocities of the actuated wheels; $\boldsymbol{\tau}(t) \in \Re^2$ is a vector of the control torques applied to the actuated wheels; $\boldsymbol{D}(t) \in \Re^2$ stands for the external disturbances which are bounded; r and b are defined in Fig. 1; $\boldsymbol{A}(\theta(t),\boldsymbol{v}(t)) \in \Re^2$ is a nonlinear vector which is continuous in $\theta(t)$ and $\boldsymbol{v}(t)$; $\boldsymbol{B}(\theta(t),\boldsymbol{v}(t)) \in \Re^{2\times 2}$ denotes the nonlinear control distribution matrix which is positive definite and continuous in $\theta(t)$ and $\boldsymbol{v}(t)$ as well. The WMR dynamics is elaborated in [19,31].

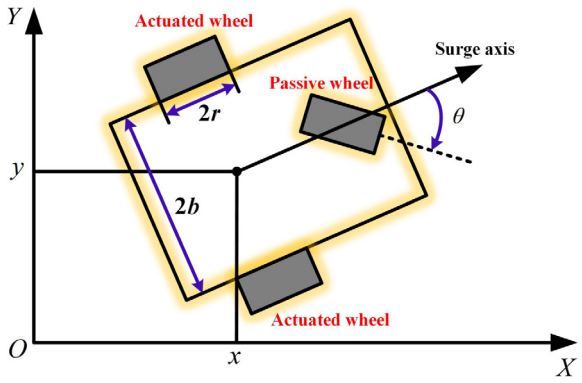

Fig. 1. Configuration of a WMR in the earth-fixed frame XOY.

2.2. Actuator PLOE faults

Consider the actuator PLOE faults as follows

$$\boldsymbol{\tau}(t) = \boldsymbol{P}(t)\boldsymbol{u}(t) = \begin{bmatrix} p_1(t) & 0 \\ 0 & p_2(t) \end{bmatrix}\begin{bmatrix} u_1(t) \\ u_2(t) \end{bmatrix}, \tag{2}$$

where $u_i(t)$ denotes the ith control signal to be designed, and $p_i(t)$ describes the efficiency of the ith actuated wheel, $i = 1, 2$. The ith actuated wheel is healthy, if $p_i(t) = 1$; it partially loses the effectiveness as $0 < p_i(t) < 1$.

Assumption 1. There exist constants $\underline{p} > 0$ and $\overline{p}$ such that [15,18,20,21]

$$\underline{p} \le p_i(t) \le 1, \quad |\dot{p}_i(t)| < \overline{p}, \quad i = 1, 2.$$

Remark 1. The WMR dynamics in (1) under the actuator PLOE faults in (2) becomes

$$\dot{\boldsymbol{v}}(t) = \boldsymbol{A}(\theta(t),\boldsymbol{v}(t)) + \boldsymbol{D}(t) + \boldsymbol{B}(\theta(t),\boldsymbol{v}(t))\boldsymbol{P}(t)\boldsymbol{u}(t), \tag{3}$$

where $\boldsymbol{B}(\theta(t),\boldsymbol{v}(t))\boldsymbol{P}(t)$ serves as the CDM. It is noted that $\boldsymbol{B}(\theta(t),\boldsymbol{v}(t))$ and $\boldsymbol{P}(t)$ are both positive-definite by definition and Assumption 1. Therefore, $\boldsymbol{B}(\theta(t),\boldsymbol{v}(t))\boldsymbol{P}(t)$ is nonsingular, which means that (3) is still controllable in the case of actuator PLOE faults. Nevertheless, $\boldsymbol{B}(\theta(t),\boldsymbol{v}(t))\boldsymbol{P}(t)$ may become an asymmetric matrix which is no longer positive-definite. It the related works on FTC under actuator PLOE faults [14–18], it is usually assumed that $(\boldsymbol{B}(\theta(t),\boldsymbol{v}(t))\boldsymbol{P}(t)) + (\boldsymbol{B}(\theta(t),\boldsymbol{v}(t))\boldsymbol{P}(t))^{\mathrm{T}}$ always remains positive-definite. This is named as the strong controllability condition of (3). However, $\boldsymbol{B}(\theta(t),\boldsymbol{v}(t))\boldsymbol{P}(t)$ may become singular or neither positive-definite nor negative-definite, because the eigenvalues of $\boldsymbol{B}(\theta(t),\boldsymbol{v}(t))\boldsymbol{P}(t)$ change with respect to $\boldsymbol{B}(\theta(t),\boldsymbol{v}(t))$. See for example

$$\boldsymbol{B} = \begin{bmatrix} 1.5 & -1.0 \\ -1.0 & 1.0 \end{bmatrix}, \quad \boldsymbol{P} = \begin{bmatrix} 1.0 & 0.0 \\ 0.0 & 0.2 \end{bmatrix},$$

$$(\boldsymbol{BP}) + (\boldsymbol{BP})^{\mathrm{T}} = \begin{bmatrix} 4.0 & 2.4 \\ 2.4 & 1.2 \end{bmatrix}.$$

The eigenvalues of $(\boldsymbol{BP}) + (\boldsymbol{BP})^{\mathrm{T}}$ are −0.0692 and 3.4692, which means that $(\boldsymbol{BP}) + (\boldsymbol{BP})^{\mathrm{T}}$ is neither positive-definite nor negative-definite. In this paper, we focus on the case where (3) does not meet the strong controllability condition and is just controllable.

2.3. Control task

The control task for the WMR is fast accurate trajectory tracking. The target trajectory is denoted by $(x_d(t), y_d(t))$.

Assumption 2. There hold $\dot{x}_d(t) \in \mathcal{L}^\infty$ and $\dot{y}_d(t) \in \mathcal{L}^\infty$.

Define the tracking errors by

$$e_x(t) = x_d(t) - x(t), \quad e_y(t) = y_d(t) - y(t). \tag{4}$$

The resulting position error is

$$e(t) = \sqrt{e_x^2(t) + e_y^2(t)}. \tag{5}$$

The requisite trajectory tracking performance is predefined by

$$e(t) < k(t) = (k_0 - k_\infty)e^{-\mu t} + k_\infty, \tag{6}$$

where μ and k_∞ are constants and quantify the tracking rate and accuracy, respectively; $k_0 > k_\infty$ is a constant; k_0, $x_d(0)$ and $y_d(0)$ meet

$$0 < e(0) < k(0). \tag{7}$$

Problem 1. For the WMR in (1) with unknown dynamics under the actuator PLOE faults in (2), design an FTC scheme such that the performance specification in (6) holds via bounded control torques.

3. Control design

In this section, a novel mixed-gain adaptation-based fault-tolerant PPC strategy is devised to solve Problem 1. On the purpose of (6), employ the following barrier function:

$$\varphi_1(t) = \ln\left(\frac{e(t)}{k(t) - e(t)}\right). \tag{8}$$

In order to handle the underactuated nature, construct a pair of auxiliary variables:

$$z_2(t) = \frac{e_x(t)\sin\theta(t)}{e(t)} - \frac{e_y(t)\cos\theta(t)}{e(t)}, \tag{9}$$

$$s_2(t) = \frac{e_x(t)\cos\theta(t)}{e(t)} + \frac{e_y(t)\sin\theta(t)}{e(t)}. \tag{10}$$

For $z_2(t)$, select a performance function as follows

$$k_2(t) = (k_{2,0} - k_{2,\infty})e^{-\mu_2 t} + k_{2,\infty}, \tag{11}$$

where $\mu_2 > 0$ and $k_{2,\infty} > 0$ are constants, and $k_{2,0} > k_{2,\infty}$ meets

$$|z_2(0)| < k_2(0) < 1. \tag{12}$$

Deploy another barrier function:

$$\varphi_2(t) = \ln\left(\frac{k_2(t) + z_2(t)}{k_2(t) - z_2(t)}\right). \tag{13}$$

Accordingly, design the following intermediate control laws:

$$\alpha_1(t) = \lambda_1 \mathrm{sign}(s_2(t))\varphi_1(t), \tag{14}$$

$$\alpha_2(t) = -\lambda_2 \mathrm{sign}(s_2(t))\varphi_2(t), \tag{15}$$

with $\lambda_1 > 0$ and $\lambda_2 > 0$ constant control gains. Let

$$z_3(t) = 0.5\alpha_1(t) + 0.5\alpha_2(t) - v_1(t), \tag{16}$$

$$z_4(t) = 0.5\alpha_1(t) - 0.5\alpha_2(t) - v_2(t). \tag{17}$$

For the intermediate errors, choose the performance functions as follows

$$k_i(t) = (k_{i,0} - k_{i,\infty})e^{-\mu_i t} + k_{i,\infty}, \quad i = 3, 4, \tag{18}$$

where $\mu_i > 0$ and $k_{i,\infty} > 0$ are constants, and $k_{i,0} > k_{i,\infty}$ fulfills

$$|z_i(0)| < k_i(0), \quad i = 3, 4. \tag{19}$$

To confine the intermediate errors, construct

$$\varphi_i(t) = \ln\left(\frac{k_i(t) + z_i(t)}{k_i(t) - z_i(t)}\right), \quad i = 3, 4. \tag{20}$$

To deal with the inputs coupling of the WMR, design

$$\rho_i(t) = \frac{k_i(t)}{k_i^2(t) - z_i^2(t)}, \quad i = 3, 4. \tag{21}$$

Let

$$\rho(t) = \begin{bmatrix} \rho_3(t) & 0 \\ 0 & \rho_4(t) \end{bmatrix}, \quad \varphi(t) = \begin{bmatrix} \varphi_3(t) \\ \varphi_4(t) \end{bmatrix}. \tag{22}$$

The final control law is formed by

$$\boldsymbol{u}(t) = \lambda_3 \|\varphi(t)\| \rho(t)\varphi(t), \tag{23}$$

where the parameter $\lambda_3 > 0$ is freely chosen, and $\|\varphi(t)\|$ aims at accommodating the actuator PLOE faults.

Remark 2. Instead of robust control schemes, adaptive estimation mechanisms and iterative learning algorithms [14–20], which are commonly adopted in the conventional FTC designs, the mixed-gain adaptation technique is combined with the decoupling PPC method to form the controller in this paper. In (23), $\|\varphi(t)\|$ is employed to automatically adapt the gains of the two control signals together, no matter when and which actuator fails. This evades the need for fault detection and isolation. Moreover, the original simplicity of PPC is preserved in the sense that the controller is free of parameter identification [4,18,19, 24,25,28,29], function approximation [5,7,8,23,26,27] and disturbance estimation [8,11], despite the independence of the dynamic model of the WMR in (1).

Remark 3. Following the existing mixed-gain adaption technique [20–22], the FTC law is in the form of

$$\boldsymbol{u}(t) = -\lambda_3 \|\rho(t)\varphi(t)\| \rho(t)\varphi(t). \tag{24}$$

Different from (24), only the barrier function vector $\varphi(t)$ is involved in our controller in (23) for gain adaption. One sees from (22) that

$$\|\rho(t)\varphi(t)\| = \sqrt{\rho_3^2(t)\varphi_3^2(t) + \rho_4^2(t)\varphi_4^2(t)},$$

$$\|\varphi(t)\| = \sqrt{\varphi_3^2(t) + \varphi_4^2(t)}.$$

Note from (21) that $\rho_i(t)$ significantly increases when $|z_i(t)|$ is less than but close to $k_i(t)$, $i = 3, 4$. In this case, $\|\rho(t)\varphi(t)\|$ is much greater than $\|\varphi(t)\|$, which means that our controller in (23) shows a significantly lower magnitude than the existing FTC law in (24). Therefore, a lower-gain adaptation scheme is employed, in comparison with [20–22].

4. Theoretical analysis

Theorem 1. *Under Assumptions 1 and 2 and the initial conditions in (7), (12) and (19), Problem 1 is addressed by the controller composed of (8)–(23).*

Proof. For uniformity, let

$$z_1(t) = e(t) - k_1(t), \quad k_1(t) = 0.5k(t). \tag{25}$$

Then, $0 < e(t) < k(t)$ implies and is implied by $|z_1(t)| < k_1(t)$. Now, we claim

$$|z_i(t)| < k_i(t), \quad i = 1, \ldots, 4, \quad \forall t \geq 0, \tag{26}$$

by seeking a contradiction. Under (7), it is obtained from (25) that $|z_1(0)| < k_1(0)$. This together with (12) and (19) yields (26) for $t = 0$. Note that the full state of the WMR, $[x(t), y(t), \theta(t), v_1(t), v_2(t)]^{\mathrm{T}}$, is uniformly continuous. It follows from Assumption 2, (6), (11) and (18) that $x_d(t)$, $y_d(t)$ and $k_i(t)$, $i = 1, \ldots, 4$, are uniformly continuous as well. Therefore, $e_x(t)$ and $e_y(t)$ in (4) and $e(t)$ in (5) remain so. One sees from (9) and (10) that

$$z_2^2(t) + s_2^2(t) = 1, \tag{27}$$

and $z_1(t)$ and $z_2(t)$ are uniformly continuous. Accordingly, $\varphi_1(t)$ in (8) and $\varphi_2(t)$ in (13) are continuous, under $0 < e(t) < k(t)$ and $|z_2(t)| < k_2(t)$. On the other hand, one sees from (11) and (12) that $k_2(t) < 1$, $t \geq 0$. Further, (27) implies $|s_2(t)| > 0$ when $|z_2(t)| < k_2(t)$. In this case, $\text{sign}(s_2(t))$ is fixed. As a result, $\alpha_1(t)$ in (14) and $\alpha_2(t)$ in (15) are continuous, as long as $0 < e(t) < k(t)$ and $|z_2(t)| < k_2(t)$. In this case, the same holds $z_3(t)$ in (16) and $z_4(t)$ in (17). The above findings manifest that if (26) is violated, then there is $t^* > 0$ so that

$$\lim_{t\to t^{*-}} |z_j(t)| = \lim_{t\to t^{*-}} k_j(t), \quad j \in \{1,\dots,4\}, \tag{28}$$

and

$$|z_i(t)| < k_i(t), \quad i = 1,\dots,4, \quad t < t^*. \tag{29}$$

Next, we suppose (28) with (29) and enumerate each scenario in (28) for justification. In what follows, the state or time dependence of the variables or functions are neglected for simplification.

Case 1: Suppose

$$\lim_{t\to t^{*-}} |z_1(t)| = \lim_{t\to t^{*-}} k_1(t), \tag{30}$$

which means that

$$\lim_{t\to t^{*-}} \frac{\mathrm{d}|z_1(t)|}{\mathrm{d}t} \geq \lim_{t\to t^{*-}} \dot{k}_1(t). \tag{31}$$

From (6) and (25), we have

$$\dot{k}_1(t) \geq 0.5\mu(k_0 - k_\infty), \quad \forall t \geq 0. \tag{32}$$

By (5) and (25), we obtain

$$\dot{z}_1 = \frac{1}{e}\left(e_x\dot{e}_x + e_y\dot{e}_y\right) - \dot{k}_1. \tag{33}$$

Differentiating (4) via (1) gives

$$\begin{cases} \dot{e}_x = \dot{x}_d - \dfrac{r}{2}(v_1 + v_2)\cos\theta, \\ \dot{e}_y = \dot{y}_d - \dfrac{r}{2}(v_1 + v_2)\sin\theta. \end{cases} \tag{34}$$

Substituting (34) together with (10) into (33) yields

$$\dot{z}_1 = \frac{1}{e}(e_x\dot{x}_d + e_y\dot{y}_d) - \dot{k}_1 - \frac{r}{2}(v_1 + v_2)s_2. \tag{35}$$

From (14)–(17), there exists

$$v_1 + v_2 = \lambda_1 \text{sign}(s_2)\varphi_1 - z_3 - z_4. \tag{36}$$

Substituting (36) into (35) yields

$$\dot{z}_1 = \delta_1 - \frac{r\lambda_1}{2}|s_2|\varphi_1, \tag{37}$$

where

$$\delta_1 = \frac{1}{e}(e_x\dot{x}_d + e_y\dot{y}_d) - \dot{k}_1 + \frac{r}{2}(z_3 + z_4)s_2. \tag{38}$$

One sees from (5) and (27) that

$$\frac{|e_x|}{e} \leq 1, \quad \frac{|e_y|}{e} \leq 1, \quad |s_2| \leq 1.$$

Under (29), there holds $|z_3 + z_4| < \infty$, $t < t^*$. Substitute the above findings together with Assumption 2 and (32) into (38). Then, we get

$$|\delta_1(t)| < \infty, \quad t < t^*. \tag{39}$$

According to (30) and (37), there is

$$\lim_{t\to t^{*-}} \frac{\mathrm{d}|\dot{z}_1(t)|}{\mathrm{d}t} = \lim_{t\to t^{*-}} \left(\delta_1 \text{sign}(z_1)\right) - \lim_{t\to t^{*-}} \left(\frac{r\lambda_1}{2}|s_2|\varphi_1 \text{sign}(z_1)\right). \tag{40}$$

Rephrase (8) via (25) as follows

$$\varphi_1 = \ln\left(\frac{k_1 + z_1}{k_1 - z_1}\right). \tag{41}$$

According to (30) and (41), there holds

$$\lim_{t\to t^{*-}} \left(\varphi_1(t)\text{sign}(z_1)\right) = \lim_{t\to t^{*-}} |\varphi_1(t)| = +\infty. \tag{42}$$

Based on (12) and (29), one sees from (11) and (27) that

$$|s_2(t)| > \sqrt{1 - k_2^2(t)} \geq \sqrt{1 - k_2^2(0)} > 0, \quad t < t^*. \tag{43}$$

Inserting (39), (42) and (43) into (40) yields

$$\lim_{t\to t^{*-}} \frac{\mathrm{d}|\dot{z}_1(t)|}{\mathrm{d}t} = -\infty. \tag{44}$$

Now, we arrive at a contradiction between (31) and (44) as a result of (32). Accordingly, (30) is invalid. Instead, there is a constant $o_1 > 0$ so that

$$|z_1(t)| \leq k_1(t) - o_1 < k_1(t), \quad t < t^*. \tag{45}$$

Case 2: Consider

$$\lim_{t\to t^{*-}} |z_2(t)| = \lim_{t\to t^{*-}} k_2(t), \tag{46}$$

which necessitates

$$\lim_{t\to t^*} \frac{\mathrm{d}|z_2(t)|}{\mathrm{d}t} \geq \lim_{t\to t^*} \dot{k}_2(t). \tag{47}$$

It follows from (11) that

$$\dot{k}_2(t) \geq 0.5\mu_2(k_{2,0} - k_{2,\infty}), \quad t \geq 0. \tag{48}$$

Differentiating (9) via (5) and (10) yields

$$\dot{z}_2 = \frac{1}{e}\left(\dot{e}_x \sin\theta - \dot{e}_y\cos\theta\right) - \frac{z_2\dot{e}}{e} + \frac{r}{2b}(v_1 - v_2)s_2. \tag{49}$$

It follows from (16) and (17) that

$$v_1 - v_2 = -\lambda_2 \text{sign}(s_2)\varphi_2 - z_3 + z_4. \tag{50}$$

Substituting (50) into (49) yields

$$\dot{z}_2 = \delta_2 - \frac{r\lambda_2}{2b}|s_2|\varphi_2, \tag{51}$$

where

$$\delta_2 = \frac{1}{e}\left(\dot{e}_x \sin\theta - \dot{e}_y\cos\theta\right) - \frac{z_2\dot{e}}{e} + \frac{r}{2b}(z_4 - z_3)s_2. \tag{52}$$

Under (46), we further get

$$\lim_{t\to t^{*-}} \frac{\mathrm{d}|\dot{z}_2(t)|}{\mathrm{d}t} = \lim_{t\to t^{*-}} \left(\delta_2 \text{sign}(z_2)\right) - \lim_{t\to t^{*-}} \left(\frac{r\lambda_2}{2b}|s_2|\varphi_2 \text{sign}(z_2)\right). \tag{53}$$

Due to (41) and (45), there holds $|\varphi_1| < \infty$ for $t < t^*$. Therefore, $\dot{e}_x$ and $\dot{e}_y$ in (34) with (36) keep bounded for $t < t^*$. Note that (45) implies by (25) that $1/e < \infty$ on $[0, t^*)$. As a result, from (33), we know $|\dot{e}| < \infty$, $t < t^*$. Substituting these findings in conjunction with (27) and (29) into (52) yields

$$|\delta_2(t)| < \infty, \quad t < t^*. \tag{54}$$

From (13) and (46), there holds

$$\lim_{t\to t^*} \text{sign}(z_2)\varphi_2(t) = +\infty. \tag{55}$$

Inserting (43), (54) and (55) into (53) shows

$$\lim_{t\to t^*} \frac{\mathrm{d}|\dot{z}_2(t)|}{\mathrm{d}t} = -\infty. \tag{56}$$

Obviously, (56) contradicts (47) due to (48). Accordingly, (46) is impossible, and instead, there is a positive constant o_2 so that

$$|z_2(t)| \leq k_2(t) - o_2 < k_2(t), \quad t < t^*. \tag{57}$$

Case 3: It remains to examine whether or not (28) holds for $j = 3, 4$. The differential equations of (16) and (17) are lumped by

$$\dot{\boldsymbol{z}} = \boldsymbol{M}\dot{\boldsymbol{\alpha}} - \dot{\boldsymbol{v}}, \tag{58}$$

where

$$\boldsymbol{M} = \begin{bmatrix} 0.5 & 0.5 \\ 0.5 & -0.5 \end{bmatrix}, \ \boldsymbol{z} = \begin{bmatrix} z_3 \\ z_4 \end{bmatrix}, \ \boldsymbol{\alpha} = \begin{bmatrix} \alpha_1 \\ \alpha_2 \end{bmatrix}.$$

Let

$$\boldsymbol{H} = \left[\frac{z_3\dot{k}_3}{k_3}, \frac{z_4\dot{k}_4}{k_4}\right]^{\mathrm{T}}. \tag{59}$$

From (20)–(22), we have

$$\dot{\varphi} = 2\rho\dot{\boldsymbol{z}} - 2\rho\boldsymbol{H}. \tag{60}$$

Substituting (58) with (3) into (60) yields

$$\dot{\varphi} = \rho \boldsymbol{L} - 2\rho \boldsymbol{B}\boldsymbol{P}\boldsymbol{u}, \tag{61}$$

where

$$\boldsymbol{L} = 2\rho(\boldsymbol{M}\dot{\alpha} - \boldsymbol{A} - \boldsymbol{D} - 2\rho\boldsymbol{H}). \tag{62}$$

Substituting (23) into (61) gives

$$\dot{\varphi} = \rho \boldsymbol{L} - 2\lambda_3 \|\varphi\| \rho \boldsymbol{B}\boldsymbol{P}\rho\varphi.$$

Construct

$$V = \varphi^{\mathrm{T}} \boldsymbol{P} \varphi, \tag{63}$$

and there is

$$\dot{V} = 2\varphi^{\mathrm{T}} \boldsymbol{P}\dot{\varphi} + \varphi^{\mathrm{T}} \dot{\boldsymbol{P}}\varphi. \tag{64}$$

Based on Assumption 1, there holds

$$\varphi^{\mathrm{T}} \dot{\boldsymbol{P}}\varphi \le \bar{p}\|\varphi\|^2. \tag{65}$$

Note from (2) and (22) that $\boldsymbol{P}\rho = \rho\boldsymbol{P}$. There thus holds

$$\varphi^{\mathrm{T}} \boldsymbol{P}\dot{\varphi} = \varphi^{\mathrm{T}} \rho \boldsymbol{P}\boldsymbol{L} - 2\lambda_3 \|\varphi\| \varphi^{\mathrm{T}} \rho \boldsymbol{B}\boldsymbol{P}\rho\varphi. \tag{66}$$

Since $\boldsymbol{P}$ is a diagonal positive definite matrix and $\boldsymbol{B}$ is positive definite, $\boldsymbol{P}\boldsymbol{B}\boldsymbol{P}$ is also positive definite. Let λ_4 be the minimum eigenvalue of $\boldsymbol{P}\boldsymbol{B}\boldsymbol{P}$. This together with Assumption 1 enables us to scale (66) as follows

$$\varphi^{\mathrm{T}} \boldsymbol{P}\dot{\varphi} \le \|\boldsymbol{L}\| \|\rho\varphi\| - 2\lambda_3\lambda_4 \|\varphi\| \|\rho\varphi\|^2. \tag{67}$$

Substituting (65) and (67) into (64) leads to

$$\dot{V} \le -4\lambda_3\lambda_4 \|\varphi\| \|\rho\varphi\|^2 + 2\|\boldsymbol{L}\| \|\rho\varphi\| + \bar{p}\|\varphi\|^2. \tag{68}$$

Under (29), there holds

$$\frac{k_i}{k_i^2 - z_i^2} \ge \frac{k_i}{k_i^2} = \frac{1}{k_i}, \quad i = 3, 4.$$

On this basis, it follows from (18), (21) and (22) that

$$\|\rho\varphi\| \ge \sqrt{\frac{\varphi_1^2}{k_1^2} + \frac{\varphi_2^2}{k_2^2}} \ge \sqrt{\frac{\varphi_1^2}{k_1^2(0)} + \frac{\varphi_2^2}{k_2^2(0)}} \ge \lambda_5 \|\varphi\|, \ t < t^*, \tag{69}$$

with $\lambda_5 = \max\{k_3(0), k_4(0)\}$. As a result of (57), φ_2 in (13) is bounded on $[0, t^*)$. Therefore, $\dot{z}_1$ in (37) and $\dot{z}_2$ in (51) are bounded for $t < t^*$. Then, (36) and (50) remain so, which ensures $|v_i| < \infty$, $i = 1, 2$, $t < t^*$. Note by definition that $\theta \in [0, 2\pi)$. Further, due to the continuity of $\boldsymbol{A}(\theta, v)$ with respect to θ and v, there holds $\|\boldsymbol{A}\| < \infty$, $t < t^*$. On the other hand, it follows from (18) and (29) that

$$\left| \frac{z_i \dot{k}_i}{k_i} \right| < \infty, \quad i = 1, 2, 3, 4, \quad t < t^*.$$

It is obtained from (14), (15) and (43) that

$$\dot{\alpha}_i = -\lambda_i \mathrm{sign}(s_2)\dot{\varphi}_i, \quad i = 1, 2, \quad t < t^*. \tag{70}$$

As (13), (20) and (41) show the same structure, one sees from (60) with (59) that

$$\dot{\varphi}_i = 2\rho_i \dot{z}_i - \frac{2\rho_i z_i \dot{k}_i}{k_i}, \quad i = 1, 2, \tag{71}$$

where

$$\rho_i = \frac{k_i}{k_i^2 - z_i^2}, \quad i = 1, 2.$$

Due to (45) and (57), ρ_1 and ρ_2 keep bounded for $t < t^*$. As a result, $\dot{\varphi}_i$ in (71) and $\dot{\alpha}_i$ in (70) remain so, $i = 1, 2$. The above findings along with $\boldsymbol{D} \in \mathcal{L}^\infty$ ensure $\|\boldsymbol{L}\| < \infty$, $t < t^*$, by (62). Then, denote

$$l := \sup_{t \in [0, t^*)} \|\boldsymbol{L}(t)\|. \tag{72}$$

Inserting (69) and (72) into (68) leads to

$$\dot{V} \le -\gamma_1 \|\varphi\| \|\rho\varphi\|^2 + \gamma_2 \|\rho\varphi\|^2 + \gamma_3 \|\rho\varphi\|, \quad t < t^*, \tag{73}$$

where $\gamma_1 = 4\lambda_3\lambda_4$, $\gamma_2 = \bar{p}/\lambda_5^2$ and $\gamma_3 = 2l$. It is noted that for $t < t^*$, if $\|\rho\varphi\| < 1$, then from (69) one has $\|\rho\| < 1/\lambda_5$; if $\|\rho\varphi\| \ge 1$, then there is $\|\rho\varphi\|^2 \ge \|\rho\varphi\|$, which yields by (73) that

$$\begin{aligned} \dot{V} &\le -\gamma_1 \|\varphi\| \|\rho\varphi\|^2 + \gamma_2 \|\rho\varphi\|^2 + \gamma_3 \|\rho\varphi\|^2 \\ &= \|\rho\varphi\|^2 (-\gamma_1 \|\varphi\| + (\gamma_2 + \gamma_3)), \quad t < t^*. \end{aligned}$$

In this case, if $\|\varphi\| > \frac{\gamma_2 + \gamma_3}{\gamma_1}$, then $\dot{V} < 0$. This means by (63) that $\|\varphi\|$ is bounded. Otherwise, $\|\varphi\| \le \frac{\gamma_2 + \gamma_3}{\gamma_1}$. Based upon the above analysis, there holds $\|\varphi\| < \infty$, $t < t^*$, under both $\|\rho\varphi\| < 1$ and $\|\rho\varphi\| \ge 1$. This in turn implies by (21) and (22) that

$$|z_i| \le k_i - o_i < k_i, \quad i = 3, 4, \quad t < t^*, \tag{74}$$

where $o_i > 0$ is a constant. Obviously, a contradiction between (28) and (45), (57) and (74) happens. Accordingly, (28) is impossible, and there holds

$$|z_i(t)| \le k_i(t) - o_i < k_i(t), \quad i = 1, 2, 3, 4, \quad t \ge 0. \tag{75}$$

Obviously, (26) holds. By (25), the prescribed trajectory tracking performance in (6) is established. Due to (75), one sees from (8), (13), (20) and (21) that $\varphi_i \in \mathcal{L}^\infty$ and $\rho_j \in \mathcal{L}^\infty$, $i = 1, 2, 3, 4$, $j = 3, 4$. This guarantees $\alpha_1 \in \mathcal{L}^\infty$ in (14), $\alpha_2 \in \mathcal{L}^\infty$ in (15) and $\boldsymbol{u} \in \mathcal{L}^\infty$ in (23) with (22). Further, by (16) and (17) with (26), we have $v_i \in \mathcal{L}^\infty$, $i = 1, 2$. Based on (2) and Assumption 1, one gets $\tau \in \mathcal{L}^\infty$. □

5. Simulation study

In order to illustrate the theoretical result, a comparative simulation is conducted in this section.

5.1. Simulation setup

The WMR is modeled by (1) with the model parameters given by [19]. Let $x(0) = 4.1355$, $y(0) = 3.9355$, $\theta(0) = 0.7584$, $v_1(0) = 0$ and $v_2(0) = 0$. The control task for the WMR is to track

$$(x_d, y_d) = (5\cos(0.1t + 0.25\pi), 5\sin(0.1t + 0.25\pi)).$$

The desired transient and steady-state performance is prescribed by

$$e(t) < k(t) = 0.98e^{-0.3t} + 0.02. \tag{76}$$

The actuator PLOE faults are simulated by

$$h_1(t) = \begin{cases} 1, & \text{if } t < 20, \\ 0.3 + 0.1\sin(t), & \text{otherwise}, \end{cases}$$

$$h_2(t) = \begin{cases} 1, & \text{if } t < 40, \\ 0.4 - 0.1\cos(0.5t), & \text{otherwise}. \end{cases}$$

5.2. Effectiveness test

According to Theorem 1, a model-free control law is designed with $\lambda_1 = \lambda_2 = 5$, $\lambda_3 = 10$ and

$$k_2(t) = 0.8e^{-0.3t} + 0.1,$$

$$k_3(t) = k_4(t) = 9.5e^{-0.3t} + 0.5.$$

Its application to the WMR yields the simulation results displayed in Figs. 2–8. One observes from Figs. 2 and 3 that the WMR tracks the target trajectory and the position error remains inside the preselected performance envelop. Therefore, the performance specification is met, in spite of the actuator faults in different phrases. Figs. 4 and 5 show that both the virtual error and the intermediate errors fulfill their respective performance requirements. Figs. 7 and 8 exhibit the actuator PLOE faults and show that the control signals and the actuator outputs are both bounded. Similarly, the boundedness of the remaining state variables is depicted in Fig. 6. As predicted by Theorem 1, the simulation results validate the effectiveness of the designed controller.

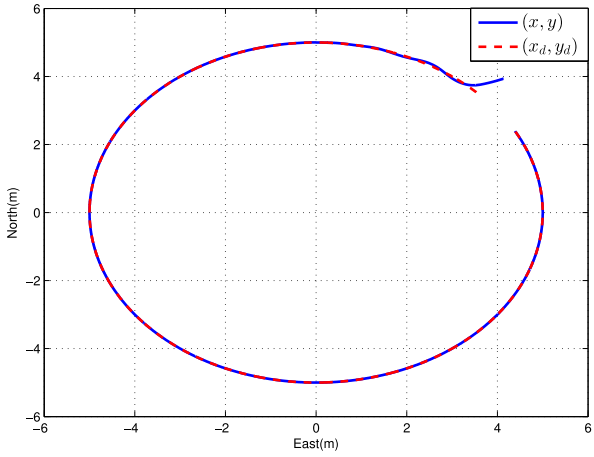

Fig. 2. The WMR path.

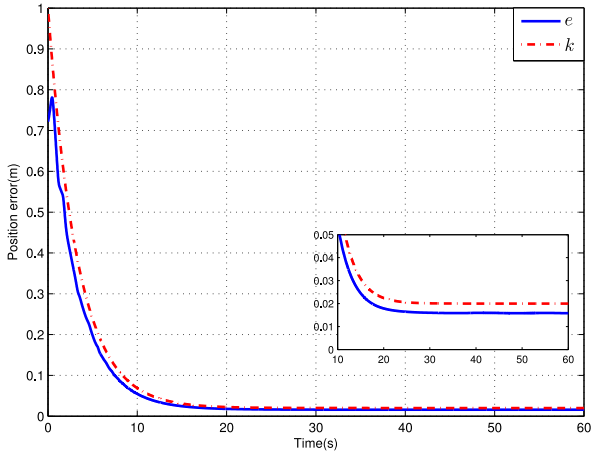

Fig. 3. The position error.

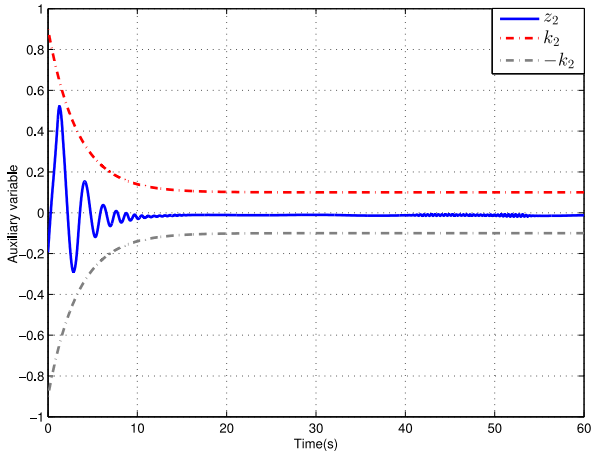

Fig. 4. The auxiliary variable.

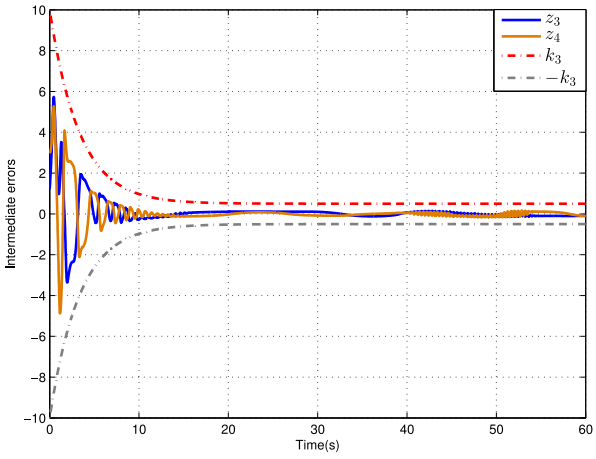

Fig. 5. The intermediate errors.

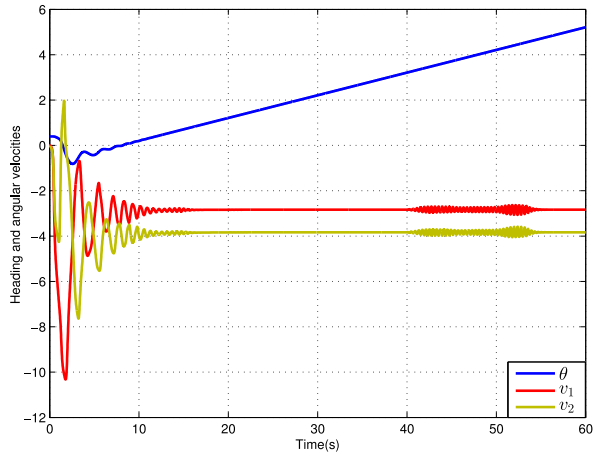

Fig. 6. The WMR heading and the angular velocities.

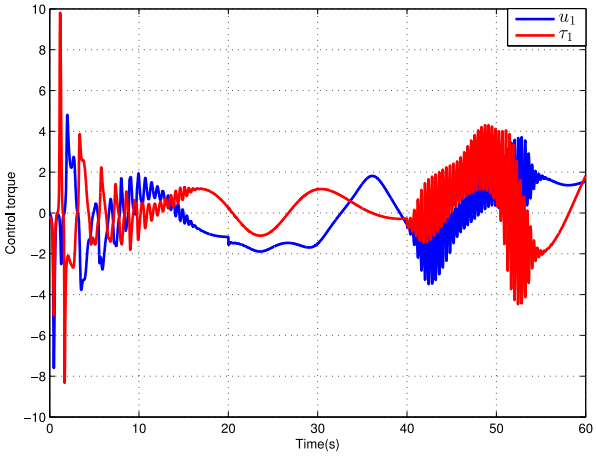

Fig. 7. The input and output of the actuator.

5.3. Comparative simulation

On the purpose of comparison, a recent fault-tolerant PPC scheme is adopted [21] with the same control objective and under the same simulation condition. Its application to the WMR yields the simulation results in Figs. 9–13. One sees from Fig. 9 that the predefined transient and steady-state tracking performance is ensured, despite the actuator faults. The similar performance guarantees hold for the auxiliary variable and the intermediate errors, as plotted in Figs. 10 and 11. However, careful inspection reveals that both the auxiliary variable and the intermediate errors fluctuate after $t = 40$s, during which the two actuators fail. This leads to significant fluctuation behaviors of

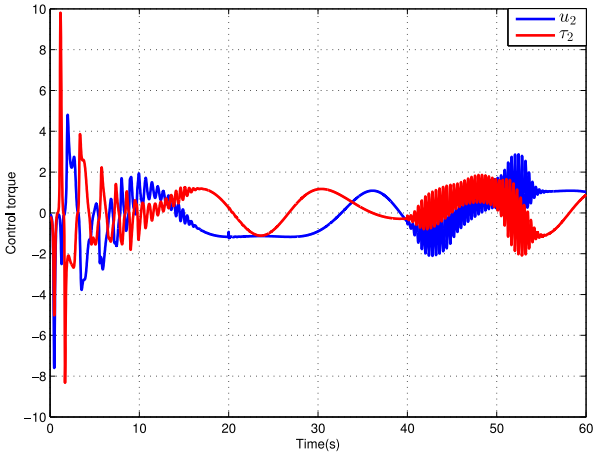

Fig. 8. The input and output of the actuator.

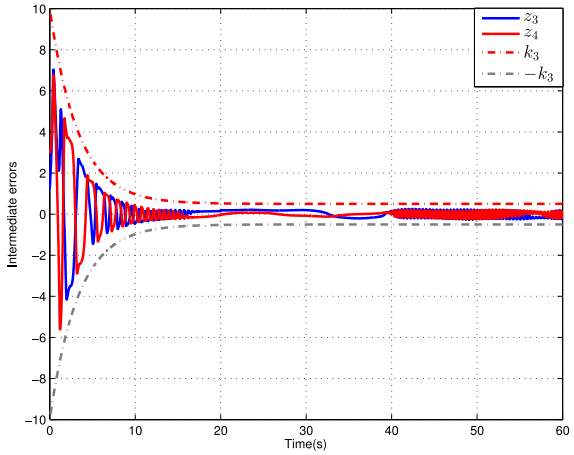

Fig. 11. The intermediate errors by the comparative controller.

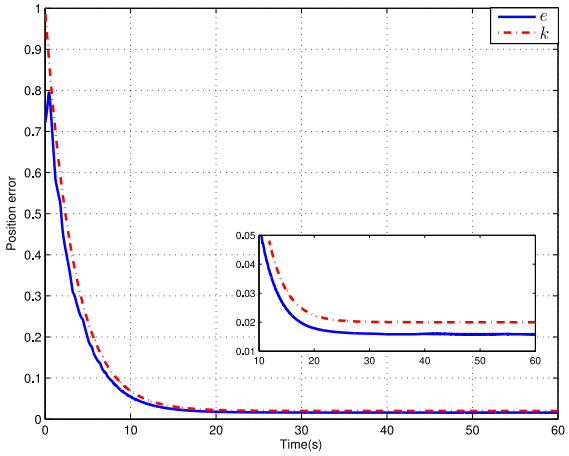

Fig. 9. The position error by the comparative controller.

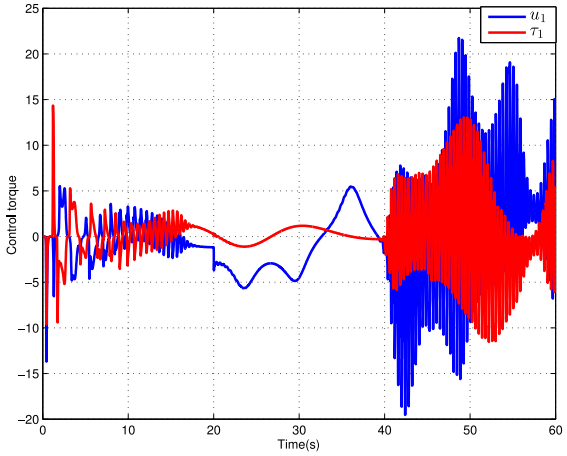

Fig. 12. The input and output of the actuator by the comparative controller.

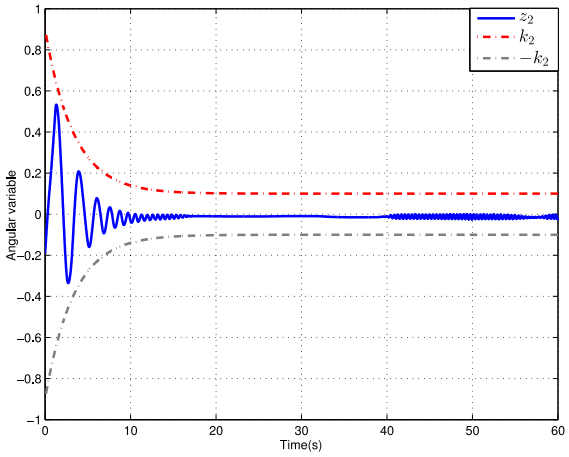

Fig. 10. The auxiliary variable by the comparative controller.

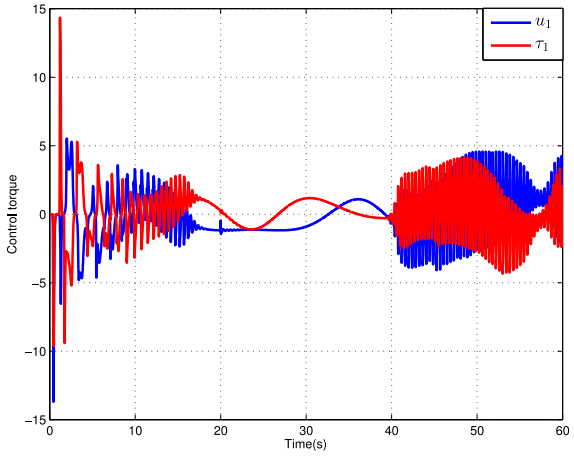

Fig. 13. The input and output of the actuator by the comparative controller.

the control signals and the actuator outputs, as depicted in Figs. 12 and 13. Such phenomenon is undesirable or even prohibited in certain practical applications. Besides, through comparison with Figs. 7 and 8, it is found that the amplitudes of the control signals and actuator outputs by the comparative FTC law become larger. Accordingly, the comparative simulation results show the advantages of our controller.

6. Conclusion

A novel mixed-gain adaption-based fault-tolerant prescribed performance control approach for the differentially driven wheeled mobile robot (WMR) subject to partial loss of effectiveness of the actuated wheels is put forward in this paper. It steers the WMR to track the

reference trajectory with the predefined rate and accuracy even in the absence of strong controllability and in the presence of external disturbances and nonparametric uncertainties. The controller exhibits a significant low control amplitude than the conventional variable gain technique and a notable low complexity with no function approximation, disturbance estimation, parameter identification, or fault diagnosis. The simulation results validate the efficacy and superiority of the proposed approach. Future work will focus on the fault-tolerant high-performance control design for the unmanned aerial vehicles.

CRediT authorship contribution statement

Jin-Xi Zhang: Writing – original draft, Methodology, Investigation. **Tianyou Chai:** Writing – review & editing, Conceptualization.

Declaration of competing interest

Jin-Xi Zhang is an associate editor for *Journal of Automation and Intelligence* and was not involved in the editorial review or the decision to publish this article. All authors declare that there are no competing interests.

Acknowledgments

This work was supported in part by the National Natural Science Foundation of China under Grants 61991404, 62103093 and 62473089, the Research Program of the Liaoning Liaohe Laboratory, China under Grant LLL23ZZ-05-01, the Key Research and Development Program of Liaoning Province of China under Grant 2023JH26/10200011, the 111 Project 2.0 of China under Grant B08015, the National Key Research and Development Program of China under Grant 2022YFB3305905, the Xingliao Talent Program of Liaoning Province of China under Grant XLYC2203130, the Natural Science Foundation of Liaoning Province of China under Grants 2024JH3/10200012 and 2023-MS-087, the Open Research Project of the State Key Laboratory of Industrial Control Technology of China under Grant ICT2024B12, and the Fundamental Research Funds for the Central Universities of China under Grants N2108003 and N2424004.

Data availability

No data was used for the research described in the article.

References

[1] R. Marino, S. Scalzi, M. Netto, Nested PID steering control for lane keeping in autonomous vehicles, Control Eng. Pract. 19 (12) (2011) 1459–1467.
[2] C. Hu, R. Wang, F. Yan, N. Chen, Output constraint control on path following of four-wheel independently actuated autonomous ground vehicles, IEEE Trans. Veh. Technol. 65 (6) (2016) 4033–4043.
[3] J.-H. Lee, W.-S. Yoo, An improved model-based predictive control of vehicle trajectory by using nonlinear function, J. Mech. Sci. Technol. 23 (2009) 918–922.
[4] J.-W. Li, Adaptive tracking and stabilization of nonholonomic mobile robots with input saturation, IEEE Trans. Autom. Control 67 (11) (2022) 6173–6179.
[5] B.S. Park, S.J. Yoo, J.B. Park, Y.H. Choi, Adaptive neural sliding mode control of nonholonomic wheeled mobile robots with model uncertainty, IEEE Trans. Control Syst. Technol. 17 (1) (2009) 207–214.
[6] X. Jin, Nonrepetitive leader–follower formation tracking for multiagent systems with LOS range and angle constraints using iterative learning control, IEEE Trans. Cybern. 49 (5) (2022) 1748–1758.
[7] M.K. Bugeja, S.G. Fabri, L. Camilleri, Dual adaptive dynamic control of mobile robots using neural networks, IEEE Trans. Syst., Man, Cybern., Syst. B, Cybern. 39 (1) (2009) 129–141.
[8] D. Chwa, Fuzzy adaptive tracking control of wheeled mobile robots with state-dependent kinematic and dynamic disturbances, IEEE Trans. Fuzzy Syst. 20 (3) (2012) 587–593.
[9] S.-L. Dai, S. He, X. Chen, X. Jin, Adaptive leader–follower formation control of nonholonomic mobile robots with prescribed transient and steady-state performance, IEEE Trans. Ind. Inform. 16 (6) (2020) 3662–3671.
[10] S.-L. Dai, K. Lu, X. Jin, Fixed-time formation control of unicycle-type mobile robots with visibility and performance constraints, IEEE Trans. Ind. Electron. 68 (12) (2021) 12615–12625.
[11] S. Chang, Y. Wang, Z. Zuo, H. Yang, Fixed-time formation control for wheeled mobile robots with prescribed performance, IEEE Trans. Control Syst. Technol. 30 (2) (2022) 844–851.
[12] W. Ding, J.-X. Zhang, P. Shi, Adaptive fuzzy control of wheeled mobile robots with prescribed trajectory tracking performance, IEEE Trans. Fuzzy Syst. 32 (8) (2024) 4510–4521.
[13] G. Tao, S. Chen, X. Tang, S.M. Joshi, Adaptive Control of Systems With Actuator Failures, Springer-Verlag, London, U.K., 2013.
[14] J.-X. Zhang, G.-H. Yang, Fault-tolerant leader-follower formation control of marine surface vessels with unknown dynamics and actuator faults, Internat. J. Robust Nonlinear Control 28 (14) (2018) 4188–4208.
[15] Y. Song, X. Huang, C. Wen, Robust adaptive fault-tolerant PID control of MIMO nonlinear systems with unknown control direction, IEEE Trans. Ind. Electron. 64 (6) (2017) 4876–4884.
[16] X. Wang, Q. Wang, C. Sun, Prescribed performance fault-tolerant control for uncertain nonlinear MIMO system using actor-critic learning structure, IEEE Trans. Neural Netw. Learn. Syst. 33 (9) (2022) 4479–4490.
[17] S. Zhou, Y. Song, Prescribed performance neuroadaptive fault-tolerant compensation for MIMO nonlinear systems under extreme actuator failures, IEEE Trans. Syst., Man, Cybern. Syst. 51 (9) (2021) 5427–5436.
[18] X. Jin, Fault tolerant nonrepetitive trajectory tracking for MIMO output constrained nonlinear systems using iterative learning control, IEEE Trans. Cybern. 49 (8) (2019) 3180–3190.
[19] X. Jin, Fault-tolerant iterative learning control for mobile robots non-repetitive trajectory tracking with output constraints, Automatica 94 (2018) 63–71.
[20] J.-X. Zhang, G.-H. Yang, Fault-tolerant output-constrained control of unknown Euler–Lagrange systems with prescribed tracking accuracy, Automatica 111 (2020) 108606.
[21] J.-X. Zhang, J. Ding, T. Chai, Fault-tolerant prescribed performance control of wheeled mobile robots: A mixed-gain adaption approach, IEEE Trans. Autom. Control 69 (8) (2024) 5500–5507.
[22] X. Gao, J.-X. Zhang, L. Hao, Fault-tolerant control of pneumatic continuum manipulators under actuator faults, IEEE Trans. Ind. Inform. 17 (12) (2021) 8299–8307.
[23] Z.-G. Hou, A.-M. Zou, L. Cheng, M. Tan, Adaptive control of an electrically driven nonholonomic mobile robot via backstepping and fuzzy approach, IEEE Trans. Control Syst. Technol. 17 (4) (2009) 803–815.
[24] J.-T. Huang, T. Van Hung, M.-L. Tseng, Smooth switching robust adaptive control for omnidirectional mobile robots, IEEE Trans. Control Syst. Technol. 23 (5) (2015) 1986–1993.
[25] B.S. Park, S.J. Yoo, J.B. Park, Y.H. Choi, A simple adaptive control approach for trajectory tracking of electrically driven nonholonomic mobile robots, IEEE Trans. Control Syst. Technol. 18 (5) (2010) 1199–1206.
[26] R. Fierro, F. Lewis, Control of a nonholonomic mobile robot using neural networks, IEEE Trans. Neural Netw. 9 (4) (1998) 589–600.
[27] L. Ding, S. Li, H. Gao, C. Chen, Z. Deng, Adaptive partial reinforcement learning neural network-based tracking control for wheeled mobile robotic systems, IEEE Trans. Syst., Man, Cybern., Syst. 50 (7) (2020) 2512–2523.
[28] K. Do, Z. Jiang, J. Pan, Simultaneous tracking and stabilization of mobile robots: an adaptive approach, IEEE Trans. Autom. Control 49 (7) (2004) 1147–1151.
[29] X. Jin, S.-L. Dai, J. Liang, Adaptive constrained formation tracking control for a tractor-trailer mobile robot team with multiple constraints, IEEE Trans. Autom. Control 68 (3) (2023) 1700–1707.
[30] J.-W. Zhu, J. Wu, Y. Feng, D. Zhang, W.-A. Zhang, L. Yu, Performance-guaranteed fault reconstruction for mobile robots via a two-dimensional gain-regulation mechanism, IEEE-ASME Trans. Mechatron. 27 (1) (2022) 169–179.
[31] K.D. Do, Formation tracking control of unicycle-type mobile robots with limited sensing ranges, IEEE Trans. Control Syst. Technol. 16 (3) (2008) 527–538.

Jin-Xi Zhang (Member, IEEE) received the B.S. degree in automation and the Ph.D. degree in control theory and control engineering from Northeastern University, Shenyang, China, in 2014 and 2020, respectively.

From 2019 to 2020, he was a Research Fellow with the Institute for Intelligent Systems, Faculty of Engineering and the Built Environment, University of Johannesburg, South Africa. He is currently a Distinguished Associate Professor with the State Key Laboratory of Synthetical Automation for Process Industries, Northeastern University, Shenyang, China.

His research interests include nonlinear control, intelligent control, prescribed performance control, multi-agent systems, fault diagnosis and fault-tolerant control, etc. He is an Associate Editor of *International Journal of Fuzzy Systems* and *Fractal and Fractional*.

Tianyou Chai (Life Fellow, IEEE) received the Ph.D. degree in control theory and engineering in 1985 from Northeastern University, Shenyang, China, where he became a Professor in 1988. He is the founder and Director of the State Key Laboratory of Synthetical Automation for Process Industries, Northeastern University, Shenyang, China. He is a member of Chinese Academy of Engineering, IFAC Fellow and IEEE Fellow. He has served as director of Department of Information Science of National Natural Science Foundation of China from 2010 to 2018.

His current research interests include modeling, control, optimization and integrated automation of complex industrial processes. He has published more than 300 peer reviewed international journal papers. His paper titled *Hybrid intelligent control for optimal operation of shaft furnace roasting process* was selected as one of three best papers for the Control Engineering Practice Paper Prize for 2011–2013. He has developed control technologies with applications to various industrial processes. For his contributions, he has won 5 prestigious awards of National Natural Science, National Science and Technology Progress and National Technological Innovation, the 2007 Industry Award for Excellence in Transitional Control Research from IEEE Multiple-conference on Systems and Control, and the 2017 Wook Hyun Kwon Education Award from Asian Control Association.